The impact of temperature vertical structure on trajectory modeling of stratospheric water vapour

T. Wang[1,2], A. E. Dessler[1], M. R. Schoeberl[3], W. J. Randel[4], J.-E. Kim[5]

[1]{Texas A&M University, College Station, Texas}

[2]{NASA Jet Propulsion Laboratory/California Institute of Technology, Pasadena, California}

[3]{Science and Technology Corporation, Columbia, Maryland}

[4]{National Center for Atmospheric Research, Boulder, Colorado}

[5]{University of Colorado, Boulder, Colorado}

Correspondence to: Tao Wang (Tao.Wang@jpl.nasa.gov)

Abstract

Lagrangian trajectories driven by reanalysis meteorological fields are frequently used to study water vapour (H_2O) in the stratosphere, in which the tropical cold-point temperatures regulate H_2O amount entering the stratosphere. Therefore, the accuracy of temperatures in the tropical tropopause layer (TTL) is of great importance for understanding stratospheric H_2O abundances. Currently, most reanalyses, such as the NASA MERRA (Modern Era Retrospective-Analysis for Research and Applications), only provide temperatures with ~1.2 km vertical resolution in the TTL, which has been argued misses finer vertical structure in the tropopause and therefore introduce uncertainties in our understanding of stratospheric H_2O. In this paper, we quantify this uncertainty by comparing the Lagrangian trajectory prediction of H_2O using MERRA temperatures on standard model levels (*traj.MER-T*), to those using GPS temperatures in

finer vertical resolution (*traj.GPS-T*) and those using adjusted MERRA temperatures with finer vertical structures induced by waves (*traj.MER-Twave*). It turns out that using temperatures with finer vertical structure in the tropopause, trajectory model more realistically simulates the dehydration of air entering the stratosphere. But the effect on H_2O abundances is relatively minor: comparing with *traj.MER-T, traj.GPS-T* tends to dry air by ~0.1 ppmv while *traj.MER-Twave* tends to dry air by 0.2-0.3 ppmv. Despite these differences in absolute values of predicted H_2O and vertical dehydration patterns, there is virtually no difference in the interannual variability in different runs. Overall, we find that tropopause temperature with finer vertical structure has limited impact on predicted stratospheric H_2O.

1. Trajectory Model and Temperatures Used

Stratospheric water vapour (H_2O) and its feedback play an important role in regulating the global radiation budget and the climate system (e.g., Holton et al., 1995; Randel et al., 2006; Solomon et al., 2010; Dessler et al., 2013). It has been known since Brewer's seminal work on stratospheric circulation that tropical tropopause temperature is the main driver of stratospheric H_2O concentration (Brewer, 1949). As parcels approach and pass through the cold-point tropopause – the altitude at which air temperature is the coldest, condensation occurs and ice falls out, thereby regulating the parcel's H_2O concentration to local saturation level (e.g., Fueglistaler et al., 2009, and references therein). This is the dehydration process. The role of tropopause temperature variation in tropical dehydration is most apparent in the annual variation in tropical stratospheric H_2O, also known as the "tape recorder" (Mote et al., 1996).

When air crosses the tropical tropopause layer (TTL), it experiences multiple dehydrations due to encounter of lower temperatures, and the final stratospheric H_2O mixing ratio is established after air passing through the coldest temperature along its path, which sets the strong relation between cold-point tropopause and the entry level H_2O (e.g., Holton and Gettelman, 2001; Randel et al., 2004, 2006).

The details of the transport and dehydration process can be understood by performing Lagrangian trajectory simulations, which track the temperature history of a large number of individual parcels. Unlike modeling chemical tracers that depends strongly on the transport imposed (Ploeger et al., 2011; Wang et al., 2014), the simulation of H_2O is primarily constrained by tropopause temperatures. Dehydration thus primarily depends on the air parcel temperature history, and stratospheric H_2O simulations ultimately require accurate analyses of temperatures particularly in the tropopause (e.g., Mote et al., 1996; Fueglistaler et al., 2005, 2009; Liu et al., 2010; Schoeberl and Dessler, 2011; Schoeberl et al., 2012, 2013).

In this paper, we use a forward, domain-filling trajectory model to study the detailed dehydration behavior of the humidity of air parcels entering the tropical lower stratosphere. Previous analyses have demonstrated that this model can accurately simulate many aspects of the observed stratospheric H_2O (Schoeberl and Dessler, 2011; Schoeberl et al., 2012, 2013). Despite the good agreements with observations, there are clear areas of uncertainties from, for instance the accuracy of circulation fields

(Schoeberl et al., 2012), the details of the dehydration mechanisms (Schoeberl et al., 2014), the influences from convection (Schoeberl et al., 2011, 2014), and the impacts from temperature vertical structures in the TTL, etc. In this paper, we investigate uncertainties introduced by the last one – the effect of vertical structures of temperatures.

This is accomplished by comparing trajectory results from using NASA Modern Era Retrospective-Analysis for Research and Applications (MERRA) (Rienecker et al., 2011) temperatures on standard model levels, to using temperatures with finer vertical structures, which include GPS temperatures in finer vertical resolution and the MERRA temperatures adjusted to account for finer vertical structure induced by waves (Kim and Alexander, 2013). This will help us to further understand the importance of the vertical structure of tropopause temperatures in dehydrating air entering the stratosphere.

2. Trajectory Model and Temperatures Used

2.1 Trajectory model

The trajectory model used here follows the details described in Schoeberl and Dessler (2011) with parcel positions integrated using the Bowman trajectory code (Bowman, 1993; Bowman et al., 2013). This model has been proven capable of simulating stratospheric H_2O and its long-term variability (Schoeberl and Dessler, 2011; Schoeberl et al., 2012, 2013; Dessler et al, 2014), modeling chemical tracer transport in the lower stratosphere (Wang et al., 2014), and studying the stratospheric air age spectrum (Ray et al., 2014). Because of the overly dispersive behavior of kinematic trajectories (e.g., Schoeberl et al., 2003; Liu et al., 2010; Ploeger et al., 2010; Schoeberl and Dessler,

93 2011), we perform diabatic trajectories using isentropic coordinates, in which the vertical
94 velocity is the potential temperature tendency converted from the diabatic heating rates
95 via the thermodynamic equation (e.g., Andrews et al., 1987). Here we used total heating
96 rates, which include heating due to long-wave and short-wave radiation, moist physics,
97 vertical diffusion, friction drag, etc.
98
99 The parcel initiation level is chosen to be the 370-K isentrope, which is above the level of
100 zero radiative heating (~355-365 K, Gettelman and Forster, 2002) but below the tropical
101 tropopause (~375–380 K) in the tropics. Every day, parcels are initialized on equal-area
102 grids covering 40^{o}N–40^{o}S and advected forward in time by reanalysis winds. At the end
103 of each day, any parcels that have descended below the 345 K (~250 hPa or ~10 km)
104 level are removed since in most cases they have entered the troposphere. The upper
105 boundary is chosen to be 2200 K isentrope (~1 hPa or ~50 km) to cover the entire
106 stratosphere. Parcels are initialized and added to the ensemble consecutively on every day
107 and the combined set of parcels is then advected forward. This process is repeated over
108 the entire integration period so that after 2-3 years the stratospheric domain is filled up
109 with parcels – this is the concept of domain-filling, which guarantees a robust statistics.
110
111 H_2O is conserved along the trajectories, except when saturation occurs; in that case,
112 excess H_2O is instantaneously removed from the parcel to keep the relative humidity with
113 respect to ice from exceeding 100%. This is sometimes referred as “instant dehydration”
114 (e.g., Schoeberl et al., 2014), which ignores detailed microphysics but has shown to
115 simulate many features of H_2O in the lower stratosphere (e.g., Fueglistaler et al., 2005;

Jensen and Pfister, 2004; Gettelman et al., 2002). We chose the 100% saturation level because 1) different saturation levels offset the simulated H_2O constant values but with identical interannual variability; and 2) the focus of the paper is to investigate the uncertainty introduced by using different temperatures, which would be the same as long as we keep the same criteria for different runs.

In addition to H_2O, we also carry methane (CH_4) concentration for each parcel. We initiate CH_4 values increased from 1.76 ppmv in 2006 to 1.83 ppmv in 2013. As described in Schoeberl and Dessler (2011), we use photochemical loss rates supplied from Goddard two-dimensional stratospheric chemistry model (Fleming et al., 2007) to convert each methane molecule into two molecules of H_2O (Dessler et al., 1994). Noted that our analysis focus on the tropical lower stratosphere, where methane oxidation has little impacts on the total H_2O abundances (Fig. 6 in Schoeberl et al., 2012).

Along each trajectory, we locate the point where air experiences the coldest temperature as the final dehydration point (FDP), which determines the stratosphere entry level H_2O mixing ratio (FDP H_2O) for that trajectory. As will be shown below, the entry level H_2O predicted by the trajectory model is affected by the vertical structures in temperature field.

2.2 Temperature datasets

In this paper, we use MERRA (Rienecker et al., 2011) circulation to advect parcels. This includes horizontal wind components and total diabatic heating rates. As shown in

139 Schoeberl et al. (2012, 2013), trajectory model driven by this reanalysis yields excellent
140 estimates of H_2O compared to observations by the Aura Microwave Limb Sounder
141 (MLS) (Read et al., 2007).
142
143 Driven by the same circulation, trajectory runs using three different temperature datasets
144 are compared to quantify the uncertainties induced by different vertical structures in
145 temperatures: 1) using MERRA standard temperatures on model levels (MER-T),
146 denoted as *traj.MER-T*; 2) using GPS radio occultation (RO) temperatures (GPS-T),
147 denoted as *traj.GPS-T*; and 3) using MERRA temperatures adjusted to have finer vertical
148 structures induced by waves (MER-Twave) (Kim and Alexander, 2013), denoted as
149 *traj.MER-Twave*. Note that MERRA does not assimilate GPS observations, which makes
150 the two temperature datasets independent from each other. Trajectory runs with the three
151 different temperature datasets are summarized in Table 1.
152
153 **2.2.1 GPS temperature**
154 Owing to its high vertical resolution, GPS temperature profiles capture the cold-point
155 tropopause with high accuracy. In this paper we use GPS wet profile (wetPrf) retrieved at
156 100-m vertical resolution using a one-dimensional variational technique based on
157 ECMWF analysis. The wetPrf and GPS Atmospheric Profile (atmPrf, derived assuming
158 no water vapor in the air) temperatures are essentially the same in 200-10 hPa but below
159 200 hPa the errors in atmPrf could be as high as ~ 3 K due to neglect of water vapour
160 (Das and Pan, 2014). Despite being retrieved at 100-m resolution, the actual vertical
161 resolution ranges from 0.5 km in the lower troposphere to ~1 km in the middle

atmosphere (Kursinski et al., 1997).

The GPS radio occultation (RO) technique makes the data accuracy independent of platforms. That makes the biases among different RO payloads could be as low as 0.2 K in the tropopause and stratosphere (Ho et al., 2009). Therefore, to compensate the relatively lower horizontal resolution (relative to that of reanalysis), we include GPS RO from all platforms. This include the Constellation Observing System for Meteorology, Ionosphere, and Climate (COSMIC) (Anthes et al., 2008), the CHAllenging Minisatellite Payload (CHAMP) satellite (Wickert et al., 2001), the Communications/Navigation Outage Forecasting System (CNOFS), the Gravity Recovery And Climate Experiment (GRACE) twin satellites (Beyerle et al., 2005), the Meteorological Operational Polar Satellite–A (MetOp-A), the Satellite de Aplicaciones Cientifico-C (SACC) satellite (Hajj et al., 2004), and the TerraSAR-X (TerraSAR-X). There are ~2000-3500 profiles per day, mostly from COSMIC, with ~700-1100 profiles of these in the tropics.

Each day, GPS temperature profiles are binned to 200-m vertical resolution. Horizontally, we grid data into 2.5x1.25 (longitude by latitude) grids with 2-D Gaussian function weighting. This gridded dataset has been successfully used in diagnosing many detailed features of tropopause inversion layer (Gettelman and Wang, 2015). We use over 7 years of GPS data available from July 2006 to December 2013, and the trajectory run using it is denoted as *traj.GPS-T*.

Fig. 1 shows a snapshot of the 100-hPa GPS raw (panel a) and gridded (panel b)

185 temperature on January 1st, 2010, compared with MERRA temperature (panel c). It
186 demonstrates that the gridded GPS temperature captures most of the features, although
187 some detailed structure might be lost due to its relatively sparse sampling.
188
189 Fig. 2 shows the GPS and MERRA temperatures in the TTL (panel a) and their
190 differences (GPS–MERRA) (panel b, extended to 31 hPa) averaged over the deep tropics
191 ($18^oS–18^oN$) during the GPS period. Here, we examine the values at the MERRA model
192 levels (large dots) as well as MERRA in-between levels (small dots), where both GPS
193 and MERRA temperatures are linearly interpolated to the same pressure levels. It shows
194 that on average GPS is at most ~0.4 K colder than MERRA around the cold-point
195 tropopause, where temperature is ~193 K at ~93 hPa (in-between MERRA coarse levels).
196 This translates to at most a 0.4 ppmv wet bias in the entry level of stratospheric H_2O,
197 assuming 100% saturation level in our model. Note that the GPS temperatures at
198 MERRA levels 100 and 85 hPa could be lower than that in MERRA if we average over
199 $10^oS–10^oN$, but it does not change the fact that MERRA is always warm biased around
200 the cold-point tropopause.
201

202 **2.2.2 MERRA temperature adjusted by waves**

203 Wave-induced disturbances on tropopause temperatures are underrepresented by current
204 reanalyses (Kim and Alexander, 2013). At the reanalysis model levels, temperature
205 variability at time scales shorter than ~10 days are weaker than radiosondes observations
206 (refer Fig. 1b-d in Kim and Alexander, 2013). Those underrepresented waves include a
207 part of the spectrum of Kelvin waves, mixed Rossby-gravity waves, and gravity waves.

When using those model level temperatures in trajectory simulations, conventional interpolation in the vertical (under time-domain), either linear or higher order, further degrades temperature structures due to averaging of waves with different phases.

To overcome these limitations, a scheme developed by Kim and Alexander, based on wave amplification from radiosonde observations and frequency-domain interpolation, has been proven effective in recovering subseasonal (less than 90 days) wave-induced variability and creating wave-like vertical structures in reanalysis temperatures (refer Kim and Alexander, 2013 for more details). Applying this scheme on MERRA temperature records yields a new MERRA temperature dataset (MER-Twave) that has finer vertical structure induced by waves (refer Fig. 3 in Kim and Alexander, 2013). The trajectory simulation using this temperature dataset is denoted as *traj.MER-Twave*.

Note that we only considered the vertical structure issue, since it is by far a limiting factor in representing waves in the TTL. A large portion of TTL wave spectrum has horizontal and temporal scales much larger and longer than reanalysis resolution, therefore, temperature behaves almost linearly in-between model horizontal and temporal resolution. However, temperature does not behave linearly in vertical space due to the fact that a significant portion of TTL waves have vertical wavelengths shorter than ~4 km (see Figure S4 in supporting information of Kim and Alexander, 2015), which could make wave-induced disturbances less represented by the ~1.2 km vertical resolution in reanalyses.

The wave scheme produces both positive and negative perturbations to the MERRA temperature profiles, depending on the phase of waves. Overall, the change in temperature induced by waves is less than 2 K (Fig. 3), although in rare cases it can reach 5-7 K. Importantly, however, about 80% of the changes in cold-point temperature are negative, with the wave scheme lowering the average cold-point temperatures by ~0.35 K. It is this reduction in cold-point temperature that is responsible for the reduction in H_2O entering the stratosphere.

In our study we included both GPS and MER-Twave datasets because they have their own advantages and limitations. GPS provides sparse sampling in the tropics (only ~700-1100 profiles per day in 30^oN–30^oS), indicating a smaller variability in GPS than likely exists, but the mean temperatures are more accurate. In contrast, MER-Twave has better variability but not accurate mean, since it is designed to have similar variability to radiosondes but with mean reserved to original MER-T. In summary, the mean temperature is closer to reality in GPS than in MER-T and MER-Twave, but the temperature variability is closer to reality in MER-Twave than in MER-T and GPS. In addition, the MER-Twave is a general technique that could be applied to situations where GPS temperatures are not available (e.g., reanalyses before 2006, climate models).

2.2.3 Interpolation scheme

In our studies, we use linear interpolation to estimate the temperature between the fixed levels of temperature datasets. However, some previous analyses have used higher order interpolations, such as cubic spline (e.g., Liu et al., 2010), to make assumptions about the

254 strong curvature of temperature profiles around the cold-point tropopause. In order to
255 determine which approach is superior, we sample GPS tropical temperature profiles at
256 MERRA vertical levels and then use the two interpolation schemes to reconstruct the full
257 GPS resolution. Then we compare the minimum saturation mixing ratio from the
258 recovered profiles to the minimum calculated from the full resolution GPS profiles.
259
260 Fig. 4a shows the probability distribution of the differences between the minimum
261 saturation mixing ratio in the full-resolution GPS profile and in the two interpolation
262 schemes. On average, the linear interpolation performs better (RMS difference is 0.18
263 and 0.25 ppmv for the linear and cubic spline, respectively). Fig. 4b shows the
264 corresponding probability distribution of the difference of the pressure of this minimum,
265 and the linear interpolation does better for this metric, too (RMS difference is 5.2 and 7.2
266 hPa for the linear and the cubic spline interpolation, respectively). We have also tested
267 higher order spline interpolations and find that none produce lower RMS errors than
268 linear interpolation. Overall, cubic spline interpolation tends to underestimate cold-point
269 temperature, making the implied H_2O too dry, as noted by Liu et al., (2010). Thus, in our
270 studies we adopted linear interpolation scheme for three different trajectory runs.
271

272 ## 3. Trajectory Results

273 ### 3.1 Dehydration patterns

274 The gridded GPS temperatures are available since July 2006, so for fair comparison we
275 start all trajectory runs at that time and run them forward till the end of 2013. For each
276 model run, we calculate statistics of the final dehydration points (FDP) for all parcels
277 entering the stratosphere. We define "parcels entering the stratosphere" as parcels that

underwent final dehydration between 45°N–45°S (thus ignoring polar dehydration) and that were already at altitudes higher (pressure lower) than 90 hPa for at least six months since the last time they were dehydrated (FDP). This guarantees that parcels already crossed the cold-point tropopause (~380 K or ~100-94 hPa) and has indeed experienced the coldest temperature along its ascending paths. Averaging over 7 years minimizes the effects of interannual variability.

Fig. 5a-c compares the FDP frequency (solid lines) and the FDP H_2O (dashed lines) in different seasons among three runs. As mentioned, the FDP H_2O can be understood as the stratosphere entry level of H_2O. In all cases, it is clear that dehydration occurs almost exclusively between 110 and 60 hPa. The average FDP H_2O reaches a minimum at 85 hPa for all runs, meaning parcels dehydrated in its vicinity carry the smallest amount of H_2O into the stratosphere. The relatively high FDP H_2O above 80 hPa (just above the entry level) comes from the parcels that avoided the tropical cold trap and experienced final dehydration at higher, warmer levels of the stratosphere. Out of ~1.3 millions of parcels in the stratosphere there are only ~0.3% bypassed the cold-point tropopause, and these parcels have little impact on the stratosphere water vapour.

The FDP frequency, however, shows large differences among three runs. The run using MERRA temperature (*traj.MER-T*) yields an annual bimodal FDP maxima distinctly at 98 and 84 hPa (Fig. 5a solid black lines), close to the MERRA model levels 100.5 and 85.4 hPa, respectively. The bimodal feature comes from averages between single, prominent peaks during DJF (December-January-February, Fig. 5a, blue) and JJA (June-

July-August, Fig. 5a, red), when cold-point tropopause is close to a particular level (DJF to 85 hPa and JJA to 100 hPa) in MERRA (Fig. 5d-e black bars), as well as averages between bi-modal peaks during MAM (March-April-May, Fig. 5a, green) and SON (September-October-November, Fig. 5a, yellow), when tropopause temperature in real atmosphere fall in between the two MERRA levels (Fig. 5f red bars). The dehydration profiles implied from using the other two datasets, however, experience smoothed changes due to gradual variations of cold-point altitudes in each season (red and blue bars in Fig. 5d-f). It is clear that physically more realistic dehydrations (Fig. 5b-c) occur with using tropopause temperatures in finer vertical structures (Fig. 5d-f red and blue bars).

Note that at FDP, the coldest temperature encountered could be either at or in-between MERRA model levels, depending on the trajectory integration intervals. Suppose our trajectory integration time step is as small as seconds, then at some time steps parcels would inevitably travel to each of the MERRA model levels, and therefore the encountered coldest temperatures would always be at either of the two levels in MERRA. In another word, the bimodal FDP distribution from MERRA run (Fig. 5a) could be even more peaked when choosing smaller integration step in our trajectories. Two reasons that we didn't choose such smaller time step: 1) the wind and temperature data are only available 6-hourly or even daily (GPS) so much smaller time step introduces more uncertainties with more interpolation; and 2) considering the balance between model efficiency and computational resources.

Fig. 6 depicts the vertical distributions of normalized FDP in time (panel a-c) and

longitude (panel d-f) sectors for the three different runs. We see that the MERRA coarse model levels do not capture the variations of cold-point tropopause well during MAM and SON, resulting in discontinuous transition of FDP from DJF to MAM, and from JJA to SON (panel a). When using GPS temperatures (panel b) and MERRA temperatures adjusted to bear finer vertical structures (panel c), the dehydration patterns show continuous variations throughout the year. The bimodal feature is more emphasized in the longitudinal-vertical view (panel d), where we can also see that throughout the year the most frequent dehydrations occur over the western tropical pacific region.

3.2 Water Vapour (H_2O)

It is obvious that trajectory simulations using GPS temperatures (*traj.GPS-T*) and MERRA temperatures adjusted by waves (*traj.MER-Twave*) tend to yield more reasonable FDP patterns around the cold-point tropopause (Fig. 5a-c solid lines), although the parcels dehydrated at particular altitudes have similar amounts of H_2O in all three models (FDP H_2O, Fig. 5a-c dashed lines). A more interesting question is whether the different dehydration occurrences affect the stratospheric H_2O predicted by the trajectory model.

Fig. 7a shows the tropical (18°N–18^{o}S) H_2O profile predicted from three trajectory runs compared with MLS observations. The vertical bars in MLS indicate the MLS vertical resolutions at each of the MLS retrieval pressure levels. Here, we see clearly that the H_2O in stratosphere reflects the different cold-point temperatures in three datasets. The differences induced by temperatures with finer vertical structures are clearly shown in Fig. 7b, where we see slightly drier air expected in GPS run since GPS temperatures are

348 at most ~0.4 K lower than that of MERRA around the tropopause (Fig. 2); whereas wave
349 perturbations produce air 0.2-0.3 ppmv drier, in agreement with previous calculations
350 (e.g., Jensen et al., 2004; Schoeberl et al., 2011).
351
352 Fig. 8c also shows that comparing to *traj.MER-T*, the dry biases from using GPS
353 temperatures are largest during MAM and SON (0.14-0.21 ppmv on average), when the
354 real cold-point tropopause cannot be resolved by the MERRA model levels. During DJF
355 and JJA, when the cold point is near one of the two MERRA standard levels (Fig. 5d-e),
356 the differences become smaller. Thus we conclude that using GPS-T and MER-Twave
357 decreases simulated stratospheric H_2O by an average of ~0.11 ppmv and 0.28 ppmv,
358 respectively, accounting for ~2.5% and 7% changes given typical stratospheric H_2O
359 abundances of ~4 ppmv.
360
361 It is important to point out that, despite these differences in the absolute value of H_2O,
362 there is virtually no difference in the anomalies (residual from the average annual cycle).
363 In Fig. 8a we compare the time series of H_2O anomalies at 83 hPa from the three different
364 trajectory runs weighted by the MLS averaging kernels as well the MLS observations.
365 Note that the interannual variations of approximately ±0.5 ppmv in H_2O are in good
366 agreement with the interannual changes of about ±1 K in cold-point tropopause
367 temperatures (Fig. 8b) for all three different runs, further supporting that the stratospheric
368 entry level of H_2O and cold-point tropopause temperature are strongly coupled (e.g.,
369 Randel et al., 2004, 2006; Randel and Jensen, 2013). We also compared *traj.MER-T* and
370 *traj.MER-Twave* over longer period (1985-2013) and it shows almost no differences in

interannual variability, either. Clearly, for studying the interannual variability of H_2O, MERRA temperatures in coarse vertical resolution are as good as temperatures in finer vertical resolution.

4. Summary

The dehydration of air entering the stratosphere largely depends on the cold-point temperature around the tropopause. This may not be represented accurately by reanalyses due to their relatively coarse vertical resolution that reports coarser vertical structure in temperature. To investigate the impacts of this, we compare trajectory results from using standard MERRA temperatures at coarse model levels (*traj.MER-T*) to those using GPS temperatures in higher vertical resolution (*traj.GPS-T*) and those using adjusted MERRA temperatures with finer vertical structures induced by waves (*traj.MER-Twave*).

Driven by the same MERRA circulation, with 100% saturation assumption we find that on average *traj.GPS-T* dries the stratospheric H_2O prediction by ~0.1 ppmv and *traj.MER-Twave* dries by ~0.2-0.3 ppmv (Fig. 7a-b), accounting for at most ~2.5% and 7.5% changes given typical stratospheric H_2O abundances of ~4 ppmv, respectively. However, despite the differences in H_2O abundances, the interannual variability (residual from the mean annual cycle) exhibits virtually no differences, due to the strong coupling between the interannual changes of stratospheric H_2O and tropical cold-point tropopause temperatures (Fig. 8). Therefore, in terms of studying the interannual changes of stratospheric H_2O, we argue that reanalysis temperatures are more useful due to its long-term availability.

394

395 Looking at the locations of FDP, we find a bimodal distribution when using standard
396 MERRA temperatures on model levels (Figs. 5-6). This is caused by the fact that the
397 cold-point tropopause is constrained to be near the two MERRA model levels (100.5 and
398 85.4 hPa) that bracket the cold-point tropopause (Fig. 5d-f). When using the temperatures
399 with finer vertical structures, the resultant FDP patterns appear to be more physically
400 reasonable (Figs. 5a-c and Fig.6).

401

402 In this paper we perform linear interpolations for all trajectory runs. Other analyses have
403 used cubic spline interpolation owing to the strong curvature of temperature profile
404 around the cold-point tropopause. We investigate the performances of both schemes using
405 GPS temperature profiles (Sect. 2.2.3) and find that while introducing new information
406 due to its assumption in the temperature profile around the tropopause, cubic spline
407 scheme tends to generate unrealistically low cold-point temperatures due to cubic fitting.
408 Therefore, the results are not necessarily realistic and on the other hand linear
409 interpolation is overall more accurate (Fig. 4).

410

411 It is well known that TTL temperatures regulate stratospheric humidity. In this paper, we
412 have investigated one issue in our understanding of TTL temperatures — the effect of
413 finer vertical structure in tropopause temperatures — and find that it is comparatively
414 minor. This provides some confidence that the trajectory model driven by current modern
415 reanalyses is capable of depicting the stratospheric water vapour accurately.

Acknowledgements

The authors thank Kenneth Bowman, Joan Alexander, Sun Wong, and Eric Jensen for their helpful discussions and comments. This work was supported by NSF AGS-1261948, NASA grant NNX13AK25G and NNX14AF15G, and partially under the NASA Aura Science Program. This work was partially carried out during visits of Tao Wang funded by the Graduate Student Visitor Program under the Advanced Study Program (ASP) at the National Center for Atmospheric Research (NCAR), which is operated by the University Corporation for Atmospheric Research, under sponsorship of the National Science Foundation.

References

Andrews, D. G., Holton, J. R., and Leovy, C. B.: Middle Atmosphere Dynamics, Academic Press, Orlando, Florida, 489 pp, 1987.

Anthes, R. A., et al.: The COSMIC/FORMOSAT‑3 mission: Early results, Bull. Am. Meteorol. Soc., 89, 313–333, doi:10.1175/BAMS-89- 3-313, 2008.

Beyerle, G., Schmidt, T., Michalak, G., Heise, S., Wickert, J., and Reigber, Ch.: GPS radio occultation with GRACE: Atmospheric profiling utilizing the zero difference technique, Geophys. Res. Lett., 32, L13806, doi:10.1029/2005GL023109, 2005.

Bowman, K. P.: Large-scale isentropic mixing properties of the Antarctic polar vortex from analyzed winds, J. Geophys. Res., 98, 23013–23027, 1993.

Bowman, K. P., Lin, J. C., Stohl, A., Draxler, R., Konopka, P., Andrews, A., and Brunner, D.: Input data requirements Lagrangian Trajectory Models, B. Am. Meteorol. Soc., 94, 1051– 1058, doi:10.1175/BAMS-D-12-00076.1, 2013.

Brewer, A. W.: Evidence for a world circulation provided by the measurements of helium and water vapor distribution in the stratosphere, Q. J. R. Meteorol. Soc., 75, 351–363, 1949.

Das, U. and Pan, C. J.: Validation of FORMOSAT-3/COSMIC level 2 "atmPrf" global temperature data in the stratosphere, Atmos. Meas. Tech., 7, 731-742, doi:10.5194/amt-7-731-2014, 2014.

Dessler, A. E., Weinstock, E. M., Hintsa, E. J., Anderson, J. G., Webster, C. R., May, R. D., Elkins, J. W., and Dutton, G. S.: An examination of the total hydrogen budget of the lower stratosphere, Geophys. Res. Lett., 21, 2563–2566, 1994.

Dessler, A. E., Schoeberl, M. R., Wang, T., Davis, S. M., and Rosenlof, K. H.: Stratospheric water vapor feedback, P. Natl. Acad. Sci. USA, 110, 18087–18091, doi:10.1073/pnas.1310344110, 2013.

Dessler, A. E., Schoeberl, M. R., Wang, T., Davis, S. M., and Rosenlof, K. H., Vernier, J.-P.: Variations of Stratospheric Water Vapor Over the Past Three Decades, J. Geophys. Res. 119, DOI: 10.1002/2014JD021712, 2014.

Fleming, E. L., Jackman, C. H., Weisenstein, D. K., and Ko, M. K. W.: The impact of interannual variability on multidecadal total ozone simulations, J. Geophys. Res., 112, D10310, doi:10.1029/2006JD007953, 2007.

Fueglistaler, S., Bonazzola, M., Haynes, P. H., and Peter, T.: Stratospheric water vapor predicted from the Lagrangian temperature history of air entering the stratosphere in the tropics, J. Geophys. Res., 110, D08107, doi:10.1029/2004JD005516, 2005.

Fueglistaler, S., Dessler, A. E., Dunkerton, T. J., Folkins, I., Fu, Q., and Mote, P. W.: The tropical tropopause layer, Rev. Geophys., 47, RG1004, doi:10.1029/2008RG000267, 2009.

Gettelman, A. and Forster, P. M. de: Definition and climatology of the tropical tropopause layer, Journal of the Meteorological Society of Japan, 80:4B, 911-924, 2002.

Gettelman, A., Randel, W. J., Wu, F., and Massie, S. T.: Transport of water vapor in the tropical tropopause layer, Geophys. Res. Lett., edited, p. 10.1029/2001GL013818, 2002.

Gettelman, A., and Wang, T.: Structural diagnostics of the tropopause inversion layer and its evolution, J. Geophys. Res. Atmos., 120, doi:10.1002/2014JD021846, 2015.

Hajj, G. A., Ao, C. O., Iijima, B. A., Kuang, D., Kursinski, E.R., Mannucci, A. J.,

Meehan, T. K., Romans, L. J., de La Torre Juarez, M., and Yunck, T. P.: CHAMP and SAC-C atmospheric occultation results and intercomparisons, J. Geophys. Res., 109, D06109, doi:10.1029/2003JD003909, 2004.
Ho, S.-P., Goldberg, M., Kuo, Y.-H., Zou, C.-Z., and Schreiner, W.: Calibration of temperature in the lower stratosphere from microwave measurements using COSMIC radio occultation data: Preliminary results, Terr. Atmos. Ocean. Sci., 20, 87–100, 2009.
Holton, J. R., Haynes, P. H., McIntyre, M. E., Douglass, A. R., Rood, R. B., Pfister, L.: Stratosphere-troposphere exchange, Rev. Geophys., 334, 405–439, 1995.
Holton, J. R., and Gettelman, A.: Horizontal transport and the dehydration of the stratosphere, Geophys. Res. Lett., 28(14), 2799–2802, doi:10.1029/2001GL013148, 2001.
Jensen, E., and Pfister, L.: Transport and freeze-drying in the tropical tropopause layer, J. Geophys. Res., 109, D02207, doi:10.1029/2003JD004022, 2004.
Kim, J.-E., and Alexander, J. M.,: A new wave scheme for trajectory simulations of stratospheric water vapor, Geophys. Res. Lett., 40, 5286–5290, doi:10.1002/grl.50963, 2013.
Kim, J.-E., and Alexander, J. M.,: Direct impacts of waves on tropical cold point tropopause temperature, Geophys. Res. Lett., doi:10.1002/2014GL062737, 2015.
Kursinski, E. R., Hajj, G. A., Schofield, J. T., Linfield, R. P., and Hardy, K. R.: Observing Earth's atmosphere with radio occultation measurements using the Global Positioning System, J. Geophys. Res., 102(D19), 23429–23465, doi:10.1029/97JD01569, 1997.
Liu, Y. S., Fueglistaler, S., and Haynes, P. H.: Advection-condensation paradigm for stratospheric water vapor, J. Geophys. Res., 115, D24307, doi:10.1029/2010jd014352, 2010.
Mote, P. W., Rosenlof, K. H., McIntyre, M. E., Carr, E. S., Gille, J. C., Holton, J. R., Kinnersley, J. S., Pumphrey, H. C., Russell III, J. M., and Waters, J. W.: An atmospheric tape recorder: the imprint of tropical tropopause temperatures on stratospheric water vapor, J. Geophys. Res., 101, 3989–4006, 1996.
Ploeger, F., Konopka, P., Gu¨nther, G., Grooß, J.-U., and Mu¨ller, R.: Impact of the vertical velocity scheme on modeling transport across the tropical tropopause layer, J. Geophys. Res., 115, doi:10.1029/2009JD012023, 2010.
Ploeger, F., Fueglistaler, S., Grooß, J.-U., Gu¨nther, G., Konopka, P., Liu, Y. S., Mu¨ller, R., Ravegnani, F., Schiller, C., Ulanovski, A., and Riese, M.: Insight from ozone and water vapour on transport in the tropical tropopause layer (TTL), Atmos. Chem. Phys., 11, 407–419, doi: 10.5194/acp-11-407-2011, 2011.
Randel, W. J., Wu, F., Oltmans, S. J., Rosenlof, K. H., Nedoluha, G. E.,: Interannual Changes of Stratospheric Water Vapor and Correlations with Tropical Tropopause Temperatures. J. Atmos. Sci., 61, 2133–2148. doi: http://dx.doi.org/10.1175/1520-0469(2004)061<2133:ICOSWV>2.0.CO;2, 2004.
Randel, W. J., Wu, F., Vömel, H., Nedoluha, G. E., and Forster, P.: Decreases in stratospheric water vapor after 2001: Links to changes in the tropical tropopause and the Brewer-Dobson circulation, J. Geophys. Res., 111, D12312, doi:10.1029/2005JD006744, 2006.
Randel, W. J. and Jensen, E. J.: Physical processes in the tropical tropopause layer and

517 their role in a changing climate, Nat. Geosci., 6, 169–176, doi:10.1038/ngeo1733,
518 2013.
519 Ray, E.A., Moore, F.L, Rosenlof, K.H, Davis, S.M., Sweeney, C., Tans, P., Wang, T.,
520 Elkins, J.W., Bönisch, H., Engel, A., Sugawara, S., T. Nakazawa and S. Aoki:
521 Improving stratospheric transport trend analysis based on SF6 and CO2
522 measurements, J. Geophys. Res. doi: 10.1002/2014JD021802, 2014.
523 Read, W. G., et al.: Aura Microwave Limb Sounder upper tropospheric and lower
524 stratospheric H2O and relative humidity with respect to ice validation, J. Geophys.
525 Res., 112, D24S35, doi:10.1029/2007JD008752, 2007.
526 Rienecker, M. M., Suarez, M. J., Gelaro, R., Todling, R., Bacmeister, J., Liu, E.,
527 Bosilovich, M. G., Schubert, S.D., Takacs, L., Kim, G.-K., Bloom, S., Chen, J.,
528 Collins, D., Conaty, A., da Silva, A., Gu, W., Joiner, J., Koster, R. D., Lucchesi, R.,
529 Molod, A., Owens, T., Pawson, S., Pegion, P., Redder, C. R., Reichle, R., Robertson,
530 F. R., Ruddick, A. G., Sienkiewicz, M., and Woollen, J.: MERRA – NASA's modern-
531 era retrospective analysis for research and applications, J. Climate, 24, 3624–3648,
532 doi:10.1175/JCLI-D-11-00015.1, 2011.
533 Schoeberl, M. R., Douglass, A. R., Zhu, Z. X., and Pawson, S.: A comparison of the
534 lower stratospheric age spectra derived from a general circulation model and two
535 data assimilation systems, J. Geophys. Res., 108, 4113, 2003.
536 Schoeberl, M. R. and Dessler, A. E.: Dehydration of the stratosphere, Atmos. Chem.
537 Phys., 11, 8433–8446, doi:10.5194/acp-11-8433-2011, 2011.
538 Schoeberl, M. R., Dessler, A. E., and Wang, T.: Simulation of stratospheric water vapor
539 and trends using three reanalyses, Atmos. Chem. Phys., 12, 6475–6487,
540 doi:10.5194/acp-12- 6475-2012, 2012.
541 Schoeberl, M. R., Dessler, A. E., and Wang, T.: Modeling upper tropospheric and lower
542 stratospheric water vapor anomalies, Atmos. Chem. Phys., 13, 7783–7793,
543 doi:10.5194/acp-13- 7783-2013, 2013.
544 Schoeberl, M. R., Dessler, A. E., Wang, T., Avery, M. A, Jensen, E.: Cloud Formation,
545 Convection, and Stratospheric Dehydration, Earth and Space Science, DOI:
546 10.1002/2014EA000014, 2014.
547 Solomon, S., Rosenlof, K. H., Portmann, R. W., Daniel, J. S., Davis, S. M., Sanford, T. J.,
548 and Plattner, G.-K.: Contributions of stratospheric water vapor to decadal changes in
549 the rate of global warming, Science, 327, 1219–1223, 2010.
550 Wang, T., Randel, W. J., Dessler, A. E., Schoeberl, M. R., and Kinnison, D. E.: Trajectory
551 model simulations of ozone (O_3) and carbon monoxide (CO) in the lower
552 stratosphere, Atmos. Chem. Phys., 14, 7135-7147, doi:10.5194/acp-14-7135-2014,
553 2014.
554 Wickert, J., Reigber, C., Beyerle, G., Ko¨nig, R., Marquardt, C., Schmidt, T., Grundwaldt,
555 L., Galas, R., Meehan, T. K., Mel- bourne, W. G., and Hocke, K.: Atmosphere
556 sounding by GPS radio occultation: First results from CHAMP: Geophys. Res. Lett.,
557 28, 3263–3266, 2011.

Table

Table 1. Different temperature datasets used in trajectory model.

Temperature Datasets	Availability	Horizontal Resolution Longitude x Latitude	Vertical Resolution In TTL	Trajectory Runs Denoted
MER-T	Daily*	2/3 x 1/2	~1.2 km	*traj.MER-T*
GPS-T (gridded)	Daily	2.5 x 1.25	0.2 km	*traj.GPS-T*
MER-Twave	Daily*	2/3 x 1/2	0.2 km	*traj.MER-Twave*

*These datasets are available 6-hourly, but for fair comparison with using GPS data, we used daily averages.

Figures

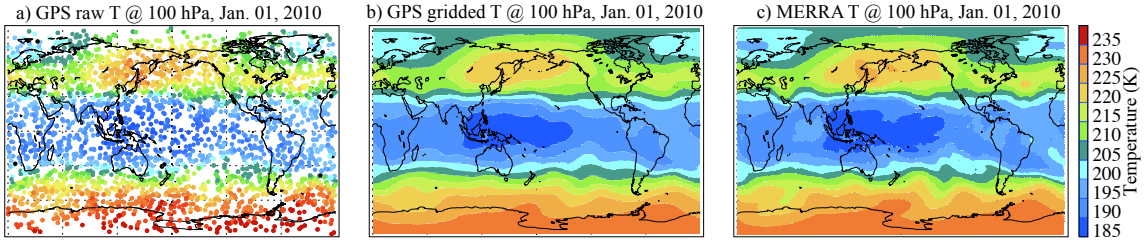

Fig. 1. (a) Comparison of temperatures from raw GPS (panel a), gridded GPS (panel b), and MERRA temperature (panel c) at 100 hPa on Jan. 1st, 2010.

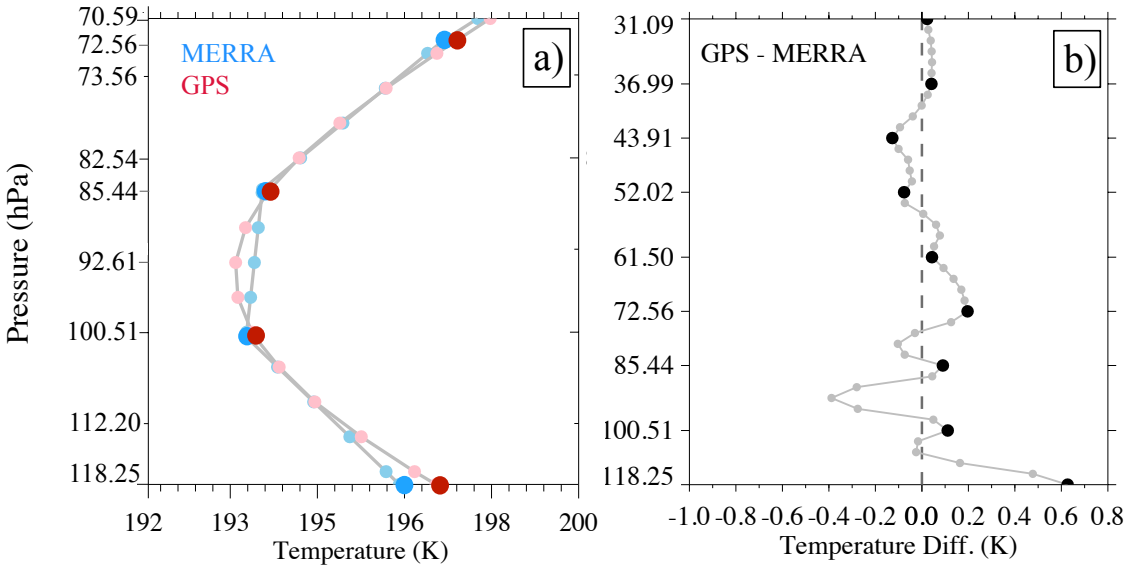

Fig. 2. (a) MERRA (blue) and GPS (red) mean temperature in TTL and (b) their differences (GPS – MERRA) extended to 31 hPa. All values are averaged over the deep tropics (18°S–18°N) in 2007-2013, with larger dots marking the MERRA model levels and small dots marking the MERRA in-between levels, where both GPS and MERRA temperatures are linearly interpolated to the same pressure levels.

567

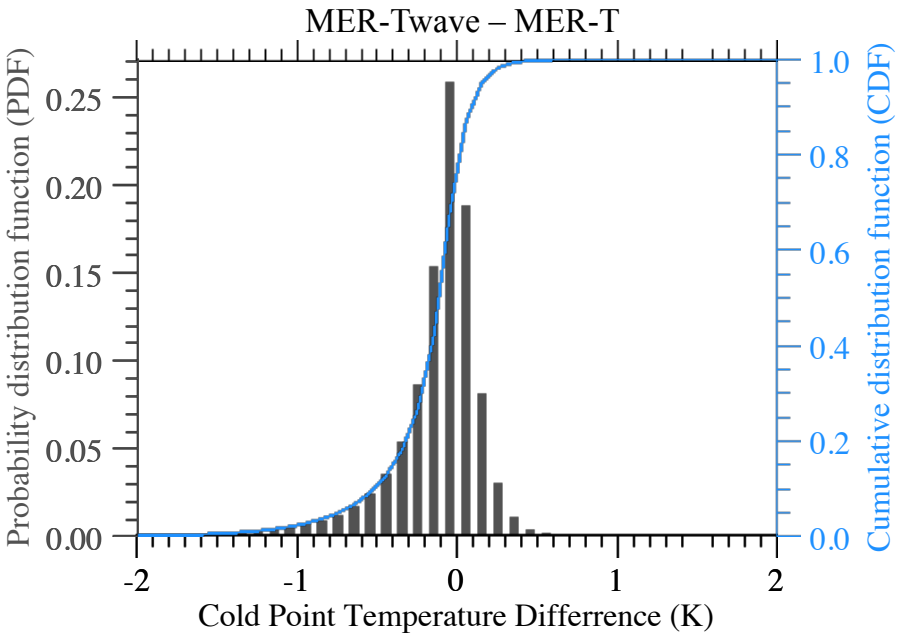

Fig. 3. Cold-Point temperature differences between MERRA adjusted by waves and MERRA (MER-Twave – MER-T) during 2007-2013. The PDF in black is plotted on left-y axis and CDF in blue on right-y axis.

568

569

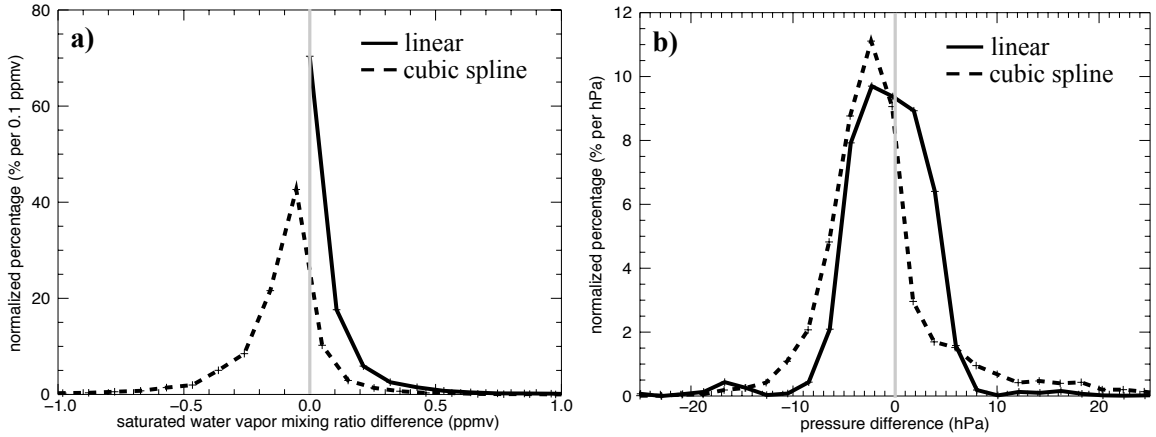

Fig. 4. PDFs of the differences between linear or cubic spline interpolations to the actual value form the GPS temperature profiles. (a) Minimum saturation mixing ratio of the profile (units are percent per 0.1 ppmv); (b) pressure of the saturation mixing ratio minimum (units are percent per hPa). The plus signs in each line mark the bin intervals.

570

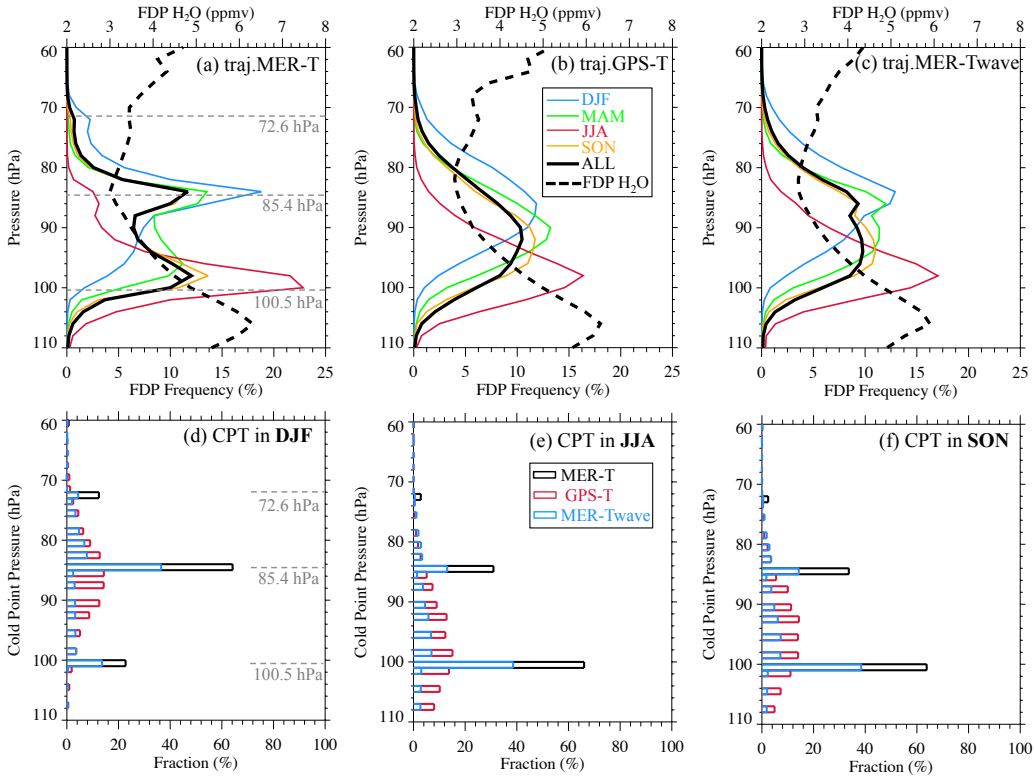

Fig. 5. Seasonal FDP vertical distributions (in %, solid lines, lower x axis) and FDP saturation mixing ratio (FDP H_2O, i.e., the stratosphere entry level H_2O, ppmv, dashed lines, upper x axis) from trajectory simulations using (a) MERRA temperatures, (b) GPS temperatures, and MERRA temperatures adjusted by waves (c), compared to the cold point tropopause statistics during (d) DJF, (e) JJA, and (f) SON. The FDP frequency is normalized by total FDP events, so each solid curve adds up to 100%. The MERRA model levels are marked in panels a and d.

571

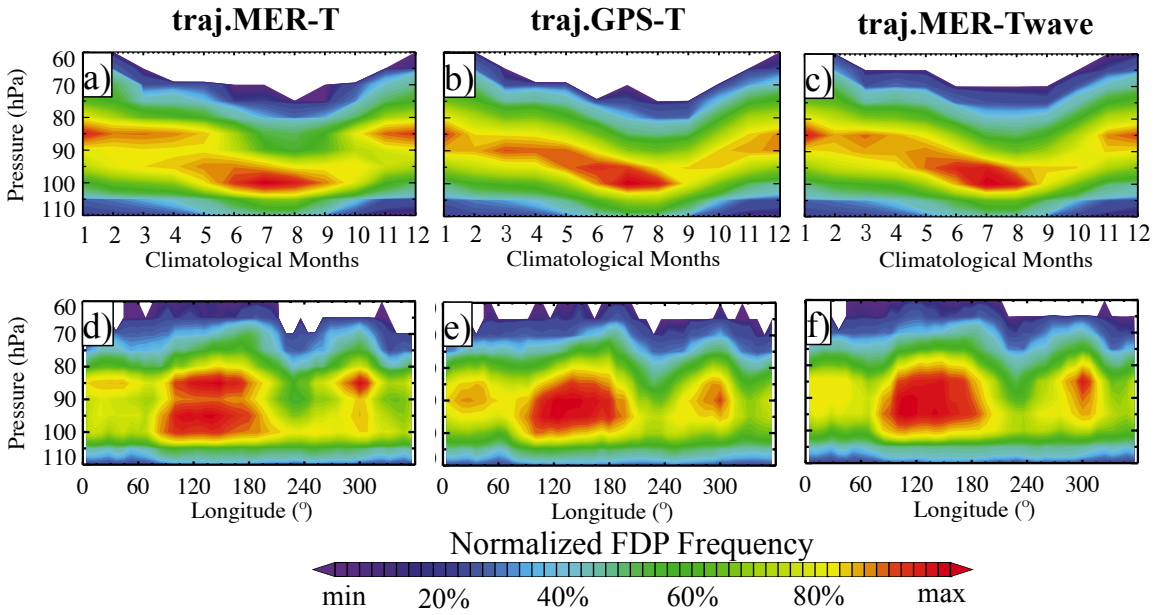

Fig. 6. Vertical distributions of normalized FDP events in time-evolutional (a-c) views among trajectory simulations by using a) MERRA temperature (*traj.MER-T*), b) GPS RO temperature (*traj.GPS-T*), and c) MERRA temperature adjusted by waves (*traj.MER-Twave*). The longitudinal variations of FDP are highlighted in panel d-f to emphasize the FDP discontinuity in *traj.MER-T*. All panels are plotted in their own range and color-coded at the same percentiles (i.e., 0, 20%, 40%, …, 100%) to compare the patterns.

572

573

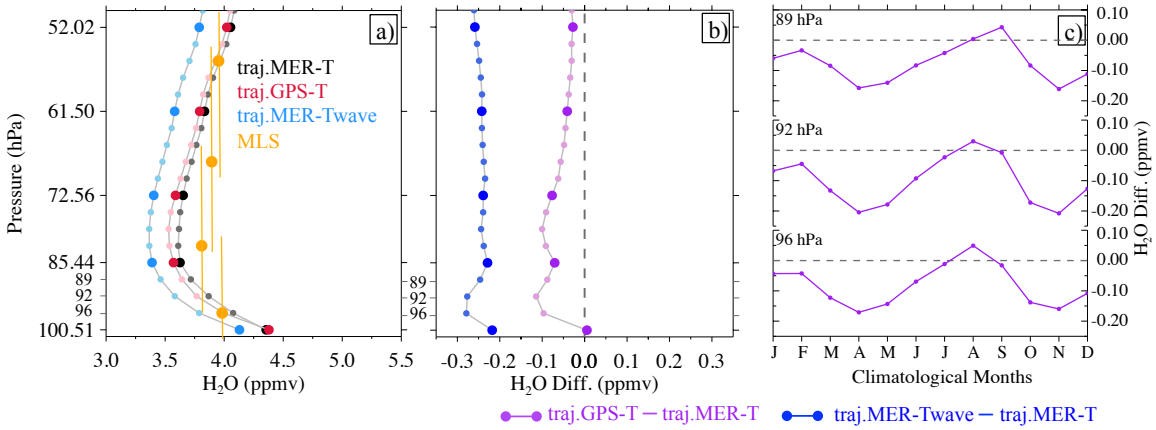

Fig. 7. (a) Trajectory predicted H_2O compared with MLS observations (the vertical bars in orange indicate the MLS vertical resolutions at each of the MLS retrieval pressure levels); (b) trajectory H_2O differences induced by waves (blue) and by using GPS temperatures (purple); (c) annual differences at 96, 92, and 89 hPa. All values are averaged over the deep tropics (18°S–18°N) in 2007-2013, with larger dots marking the MERRA model levels and small dots marking the MERRA in-between levels – those are the levels that the cold-point tropopause could have been found but not available in current MERRA vertical resolution.

574

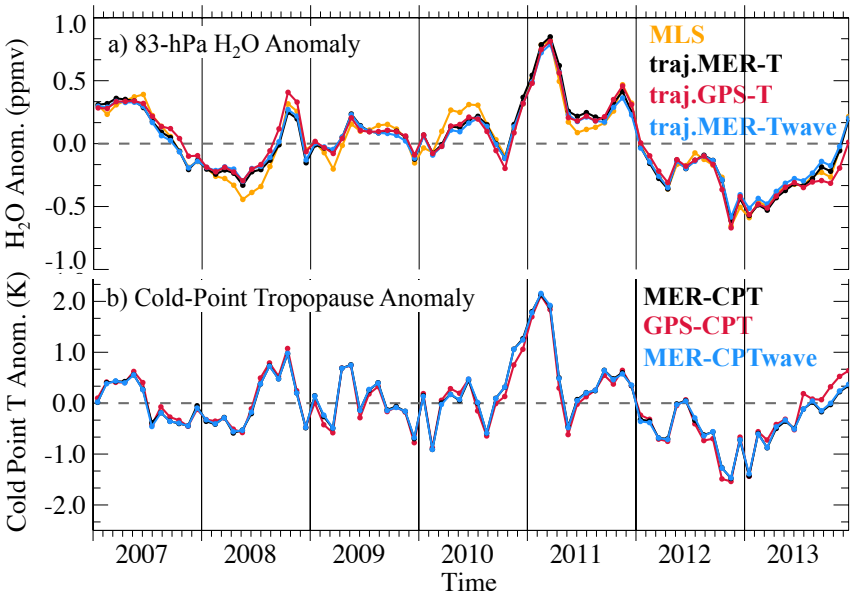

Fig. 8. (a) Trajectory simulated H_2O anomalies compared with the MLS observations; and (b) cold-point temperature anomalies from three temperature datasets. All time series are averaged over the deep tropics (18^oN-18^oS). All trajectory results in panel a are weighted by the MLS averaging kernels for fair comparison.

575